Multi-step vortex filtering for phase extraction

Alberto Aguilar,[1] **Abundio Dávila,**[1*] **and Jorge García-Márquez**[2]

[1] *Centro de Investigaciones en Óptica, A.C. Lomas del Bosque 115, CP. 37150 León, México*
[2] *LISV, Université de Versailles Saint-Quentin-en-Yvelines, 10/12 Avenue de l' Europe, 78140 Vélizy. And Laboratoire Commun de Métrologie LNE/CNAM 1, rue Gaston Boissier, 75724 Paris Cedex 15, France*

[*] *adavila@cio.mx*

Abstract: A quantized version of a continuous spiral phase filter with unitary topological charge, here denominated multi-step spiral phase filter (MSSPF), is proposed to extract phase from rotated spiral interferograms. Spiral interferograms are usually obtained from phase objects by registering the interference of its vortex filtered complex amplitude with a reference complex amplitude. The structure found in this kind of interferograms, depend on the number of steps used in the MSSPF that usually are assumed with an infinite number of steps for the continuous spiral phase filter. Reducing the number of steps of the MSSPF affects the residual phase error obtained after the phase extraction method. This error is therefore analysed here using a numerical simulation of a Mach-Zender interferometer with a MSSPF and a reduced number of steps. It is shown that, for our proposed method of rotated spiral interferograms, a residual error persists as the number of steps is increased approaching the residual error reported for the phase extraction method of single-shot spiral interferograms. Furthermore, it is shown that this novel technique can be applied without further modifications for phase contrast measurement. Experimental results show similar performance of this phase extraction technique, when compared to the results obtained with a commercial interferometer and with the numerical simulations.

OCIS codes: (120.5050) Phase Measurement; (050.4865) Optical vortices; (230.6120) Spatial light modulators.

References and links

1. S. N. Khonina, V. V. Kotlyar, M. V. Shinkaryev, V. A. Soifer, and G. V. Uspleniev, "The phase rotor filter" J. Mod. Opt. **39**, 1147-1154 (1992).
2. J. A. Davis, D. E. McNamara, D. M. Cottrell, and J. Campos, "Image processing with the radial Hilbert transform: theory and experiments" Opt. Lett. **25**, 99-101 (2000).
3. K. Crabtree, J. A. Davis, and I. Moreno, "Optical processing with vortex-producing lenses" Appl. Opt. . **43**, 1360-1367 (2004).
4. S. Fürhapter, A. Jesacher, S. Bernet, and M. Ritsch-Marte, "Spiral interferometry" Opt. Lett. **30**, 1953-1955 (2005).
5. A. Jesacher, S. Fürhapter, S. Bernet, and M. Ritsch-Marte, "Shadow effects in spiral phase contrast microscopy" Phys. Rev. Lett. **94**, 233902 (2005).
6. P. Bouchal and Z. Bouchal, "Selective edge enhancement in three-dimensional vortex imaging with incoherent light" Opt. Lett. **37**, 2949-2951 (2012).
7. M. K. Sharma, J. Joseph, and P. Senthilkumaran, "Selective edge enhancement using shifted anisotropic vortex filter" J. Opt. **42**, 1-7 (2012).

#204866 - $15.00 USD Received 27 Jan 2014; revised 13 Mar 2014; accepted 15 Mar 2014; published 2 Apr 2014

8. M. K. Sharma, J. Joseph, and P. Senthilkumaran, "Directional edge enhancement using superposed vortex filter" Opt. Laser Technol. 16 (2013).
9. S. Bernet, A. Jesacher, F. Severin, C. Maurer, and M. Ritsch-marte, "Quantitative imaging of complex samples by spiral phase contrast microscopy" Opt. Express **14**, 3792-3805 (2006).
10. C. Maurer, A. Jesacher, S. Bernet, and M. Ritsch-Marte, "What spatial light modulators can do for optical microscopy" Laser Photonics Rev. **5**, 81101 (2011).
11. C. S. Guo, D. M. Xue, Y. J. Han, and J. Ding, "Optimal phase steps of multi-level spiral phase plates" Opt. Commun. **268**, 235-239 (2006).
12. M. Baranek and Z. Bouchal, "Rotating vortex imaging implemented by a quantized spiral phase modulation" J. Europ. Opt. Soc. Rap. Public. **8**, 130171-130178 (2013).
13. E. Rueda, D. Muñetón, J. A. Gómez, and A. Lencina, "High-quality optical vortex-beam generation by using a multilevel vortex-producing lens" Opt. Lett. **38**, 3941-3944 (2013).
14. A. Aguilar, A. Dávila, and J. E. A. Landgrave, "Displacement measurement with multi-level spiral phase filtering in speckle interferometry" Opt. Lasers Eng. **52**, 19-26 (2014).
15. M. Servin and J. C. Estrada, "Analysis and synthesis of phase shifting algorithms based on linear systems theory" Opt. Lasers Eng. **50** 1009-1014 (2012).
16. Z. Wang and A. C. Bovik, "A universal image quality index" IEEE Signal Process. Lett. **XX**, 1-4 (2002).
17. D. Kerr, G. H. Kaufmann and G. E. Galizzi, "Unwrapping of interferometric phase-fringe maps by the discrete cosine transform" Appl. Opt. **35**,810-816 (1996).
18. K. G. Larkin, D. J. Bone, and M. A. Oldfield, "Natural demodulation of two-dimensional fringe patterns. I. General background of the spiral phase quadrature transform" J. Opt. Soc. Am. A **18**, 1862-1870 (2001).
19. A. Jesacher, S. Fürhapter, S. Bernet, and M. Ritsch-Marte, "Spiral interferogram analysis" J. Opt. Soc. Am. A **23**, 1400-1709 (2006).
20. Y. Calderón-Hermosillo, J. García-Márquez, R. Espinosa-Luna, N. Alcalá-Ochoa, V. López, A. Aguilar, E. Noé-Arias, and Y. Alayli, "Flicker in a twisted nematic spatial light modulator" Opt. Lasers Eng. **51**, 741-748 (2013).
21. J. Garcia-Marquez, V. Lopez, A. Gonzalez-Vega, and E. Noé, "Flicker minimization in an LCoS spatial light modulator" Opt. Express, **8**, 8431-8441 (2012).

1. Introduction

The initial research involving continuous vortex phase plates used as phase filters, has been established two decades ago [1], although its practical implementation had to wait until the advent of spatial light modulators (SLM) [2, 3]. It has been shown that a spiral interferogram is produced when a vortex filtered complex amplitude interferes with a reference complex amplitude. The spiral fringe patterns [4] of the interferograms can led successfully to solve the sign uncertainty by knowing the induced sense of the spirals. Further research with continuous vortex filters found some interesting applications in edge detection [5–8] and in phase contrast microscopy [9, 10].

Moreover, phase vortex can exhibit a phase stepped structure as shown in [11, 12], and the same stepped structure has allowed the generation of vortex lenses [13]. Filtering with a stepped phase vortex has been reported recently for applications of speckle interferometry [14]. Here we expand this previous research of stepped vortex filtering, using a filter with an arbitrary number of steps, and apply it for phase extraction purposes of non-speckled phase objects. The noise influence of selecting an arbitrary number of steps of the quantized phase filter is analyzed by a computer simulation of a Mach-Zender interferometer with the quantized vortex filter. Experimental results show similar performance of the proposed phase extraction technique, in terms of residual noise, when compared to the numerical simulations of the proposed technique.

2. Multi-step spiral phase filter

We define a MSSPF as a quantized version of a spiral phase filter of unitary topological charge (SPF). The spiral phase of the filter is discretized into a $p-$steps of vortex phase, such as its structure resembles a snail stair. The transfer function of the generalized MSSPF can be expressed as:

#204866 - $15.00 USD Received 27 Jan 2014; revised 13 Mar 2014; accepted 15 Mar 2014; published 2 Apr 2014

$$\mathbb{H}_p^{(n)}(u,v) = \mathrm{circ}\left(\frac{\rho}{\rho_o}\right)\exp[i\Psi_p^{(n)}(u,v)], \tag{1}$$

where (u,v) are the spatial frequency coordinates, $\rho = \sqrt{u^2+y^2}$, ρ_o is the radius of the filter in spatial frequency units, and p represents the number of the filter steps (or quadrants for $p = 4$), with the restriction that $p \in \mathbb{N}$, where $\mathbb{N}$ is the set of all natural numbers . As usual $\mathrm{circ}(\rho/\rho_o) = 1$ if $\rho \leq \rho_o$. The MSSPF depends on n, which represents the multiple combinations that the orientation of the major vortex discontinuity can represent, where $n \leq p$. Each discretized filter can have n orientations; the possible phase configuration for each MSSPF can be represented as:

$$\begin{aligned}\boldsymbol{\Psi}_p(u,v) &= \left[\Psi_p^{(1)}(u,v), \Psi_p^{(2)}(u,v), \ldots, \Psi_p^{(n)}(u,v)\right]^{\mathrm{T}} \\ &= \frac{2\pi}{p}\mathbf{R}\mathbf{q}_p(u,v),\end{aligned} \tag{2}$$

where the symbol ^{T} denotes transposition,

$$\begin{aligned}\mathbf{R} &= [r_{i,j}] \\ &= [\mathbf{r}_1, \mathbf{r}_2, \ldots, \mathbf{r}_p]^{\mathrm{T}} \\ &= \begin{pmatrix} 0 & 1 & 2 & \ldots & p-1 \\ p-1 & 0 & 1 & \ldots & p-2 \\ \vdots & & \ddots & & \vdots \\ 2 & \ldots & p-1 & 0 & 1 \\ 1 & 2 & \ldots & p-1 & 0 \end{pmatrix},\end{aligned} \tag{3}$$

and

$$\mathbf{q}_p(u,v) = [q_1(u,v),\ q_2(u,v),\ \ldots, q_j(u,v)]^{\mathrm{T}}, \tag{4}$$

here we refer to $\mathbf{q}_p(u,v)$ as the step level vector (a vector whose elements are functions), with $j \leq p$, and to $\mathbf{R}$ as the vortex rotation matrix. Notice, form Eq. (2) that the maximum phase of the MSSPF is not 2π, as for the SPF, but $\frac{2\pi(p-1)}{p}$. This implies that, the MSSPF requires less phase modulation than the spiral phase plate.

The step level function $q_j(u,v)$ is defined as:

$$q_j(u,v) = \begin{cases} 1 & \frac{2\pi(j-1)}{p} < \theta \leq \frac{2\pi j}{p}, \\ 0 & \text{otherwhise} \end{cases} \tag{5}$$

where $\theta = \tan^{-1}(v/u)$ is the angular polar coordinate. The step level function is a radial variation of the Heaviside function $H(u) = 1$ if $u > 0$ otherwise is 0. An special characteristic of the step level vector is that the sum of its components is one for all the function domain, $\sum_{j=1}^{p} q_j(u,v) = 1$.

Using Eqs. (2) and (3), Eq.(1) can be expressed as:

$$\mathbb{H}_p^{(n)}(u,v) = \mathrm{circ}\left(\frac{\rho}{\rho_o}\right)\exp\left[i\frac{2\pi}{p}\sum_{j=1}^{p} r_{n,j}q_j(u,v)\right], \tag{6}$$

taking into account that

$$r_{n,j} = r_{1,j} + n - 1 \qquad \mathrm{mod}\ p, \tag{7}$$

#204866 - $15.00 USD Received 27 Jan 2014; revised 13 Mar 2014; accepted 15 Mar 2014; published 2 Apr 2014

The n^{th} filter can be rewritten as:

$$\begin{aligned}\mathbb{H}_p^{(n)}(u,v) &= \operatorname{circ}\left(\frac{\rho}{\rho_o}\right)\exp[i\Psi_p^{(1)}(u,v)] \\ &\times \exp\left[i\frac{2\pi(n-1)}{p}\sum_{j=1}^{p}q_j(u,v)\right] \\ &= \operatorname{circ}\left(\frac{\rho}{\rho_o}\right)\exp\left[i\frac{2\pi(n-1)}{p}\right]\mathbb{H}_p^{(1)}(u,v),\end{aligned} \tag{8}$$

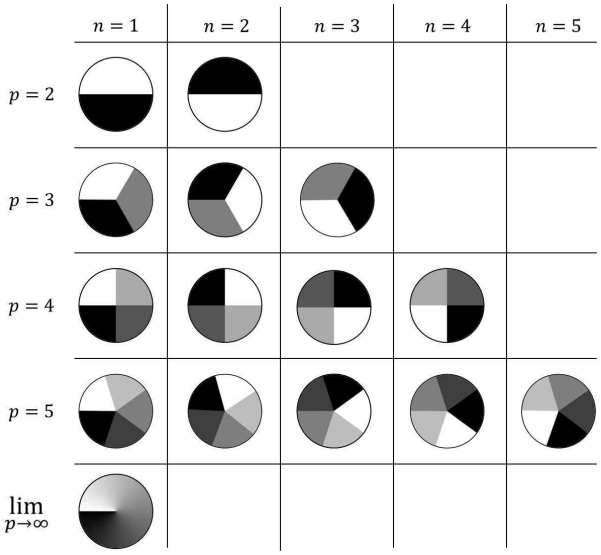

Fig. 1. Phase of the MSSPF with variation of the n and p parameters

Thus the n^{th} filter can be expressed as a combination of the filter, whose major discontinuity orientation coincides with the axis $\theta = 0$, and a multiplicative factor that only depends on n. This factor provides the effect of rotation for the different multi-steps spiral phase filters. The effect of varying the parameters p and n are sketched in Fig. 1. When p approaches to ∞ the MSSPF approach the well known spiral phase filter $\mathbb{H}_\infty^{(n)}(u,v) = \operatorname{circ}\left(\frac{\rho}{\rho_o}\right)\exp[il\theta]$, with topological charge $l = 1$. The spiral phase filter can also be quantized for different topological charges as shown in [11,13]. Nonetheless if topological charges l greater than 1 are used, the proposed approach can still be applied, except that the condition $n \leq lp$ should be met.

The convolution kernel $h_p(x_i,y_i)$ of the MSSPF has to be described in order to know the performance of the filter operation using the MSSPF. To calculate the kernel the Fourier transform has to be implemented.

$$h_p(x_i,y_i) = \mathscr{F}^{-1}\left\{\mathbb{H}_p(u,v)\right\} \tag{9}$$

where $\mathscr{F}$ and $\mathscr{F}^{-1}$ are, respectively, the forward and inverse Fourier transform operators. The computed point spread functions (PSF) of the $p-$MSSPF ($|h_p(x_i,y_i)|^2$) are shown in Fig. 2. The number of lobulus in the PSFs of the MSSPFs increases as the number of steps p grows; until it reaches the typical doughnut kernel of the spiral phase filter.

#204866 - $15.00 USD Received 27 Jan 2014; revised 13 Mar 2014; accepted 15 Mar 2014; published 2 Apr 2014

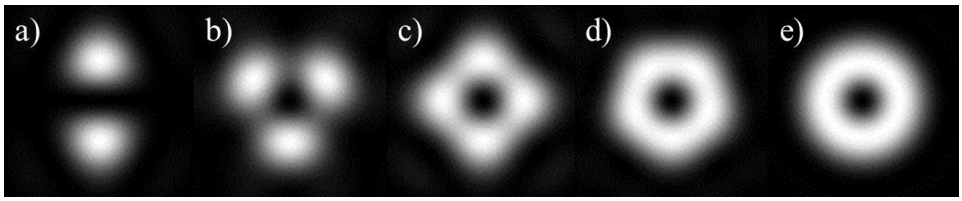

Fig. 2. Point Spread Functions of the multi-step spiral phase filter. a)$|h_2(x_i,y_i)|^2$, b)$|h_3(x_i,y_i)|^2$, c)$|h_4(x_i,y_i)|^2$, d)$|h_5(x_i,y_i)|^2$, e)$|h(x_i,y_i)|^2$

2.1. Phase extraction using multi-step spiral phase filters

Once the MSSPF was described, the filtering properties as well as the procedures for the object phase extraction are discussed. The spatial filtering operation can be represented as:

$$U_{i_p}^{(n)}(x_i,y_i) = \mathscr{F}^{-1}\left\{\mathbb{H}_p^{(n)}(u,v)\mathscr{F}\left\{U_o(x_o,y_o)P(x_o,y_o)\right\}\right\}, \tag{10}$$

where,

$$U_o(x_o,y_o) = E_o(x_o,y_o)\exp[i\varphi_o(x_o,y_o)], \tag{11}$$

and, $P(x_o,y_o)$ is the generalized pupil function. The amplitude $E_o(x_o,y_o)$ and the phase $\varphi_o(x_o,y_o)$ in Eq. (11) are the distributions from the object complex field as shown in Fig. 3. In the description it is assumed that the object is placed at the front focal plane of the Fourier transforming lens so the vignetting is neglected.

The filtering operation can be easily implemented in a $4f$ optical system, in which the MSSPF is placed in the frequency plane with coordinates (x_f,y_f) related with the spatial coordinates by $(u,v) = (x_f/\lambda f, y_f/\lambda f)$. Where λ is the light wavelength and f the focal length of the transform lens. In this system, the Fourier transform of the complex amplitude distribution $U_o(x_o,y_o)P(x_o,y_o)$, generated by coherent light transmitted from the object at the plane (x_o,y_o), and bounded by the pupil function, is obtained at the back focal plane (x_f,y_f) of the lens L_1. The MSSPF adds its phase to the propagated spectrum $G_f(u,v) = \mathscr{F}\{U_o(x_o,y_o)P(x_o,y_o)\}$ and the resulting complex amplitude is then Fourier transformed by the lens L_2, to generate the filtered wavefront in the image plane (x_i,y_i).

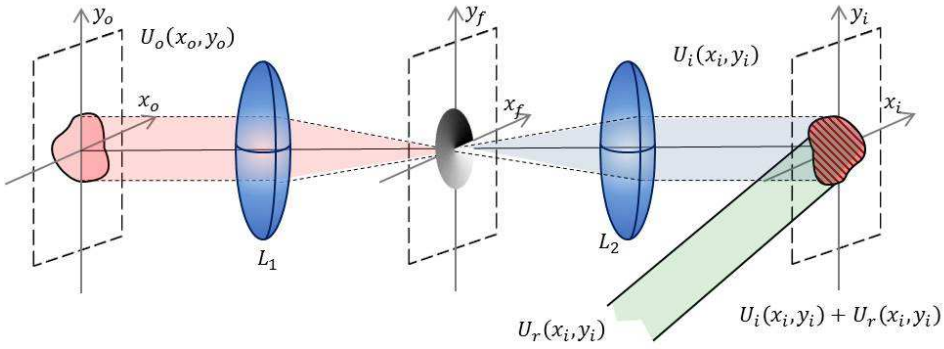

Fig. 3. Schematic diagram of a $4f$ optical correlator with a phase vortex filter represented in gray levels at the common focus to L_1 and L_2

To obtain the interference pattern in the image plane, let suppose that we add a reference wavefront $U_r(x_i,y_i)$ to the filtered wavefront $U_i(x_i,y_i)$. For simplicity, it is further assumed

#204866 - $15.00 USD Received 27 Jan 2014; revised 13 Mar 2014; accepted 15 Mar 2014; published 2 Apr 2014

that this reference beam is parallel, and incides normally to the camera CCD, with a constant amplitude E_r, then $U_r(x_i,y_i) = E_r$. The recorded interference distribution is

$$\begin{aligned} I_p^{(n)}(x_i,y_i) &= \left| U_r(x_i,y_i) + U_{i_p}^{(n)}(x_i,y_i) \right|^2 \\ &= \left| E_r + \mathscr{F}^{-1}\left\{ \mathbb{H}_p^{(n)}(u,v) G_f(u,v) \right\} \right|^2 \end{aligned} \tag{12}$$

The subindex p also appears in the intensity distribution $I(x_i,y_i)$, this means that the number of steps affect the interferogram displayed in the CCD. Eq. (12) can be rewritten using Eq. (6).

$$\begin{aligned} I_p^{(n)}(x_i,y_i) &= \left| E_r + \exp\left[i\left(\frac{2\pi(n-1)}{p} \right) \right] \right. \\ &\times \left. \mathscr{F}^{-1}\left\{ \mathbb{H}_p^{(1)}(u,v) G_f(u,v) \right\} \right|^2 \\ &= \left| E_r + \exp\left[i\left(\frac{2\pi(n-1)}{p} \right) \right] U_{i_p}^{(1)}(x_i,y_i) \right|^2 \end{aligned} \tag{13}$$

Developing the expression we can find

$$\begin{aligned} I_p^{(n)}(x_i,y_i) &= \mathscr{A}_p(x_i,y_i) \\ &+ \mathscr{B}_p(x_i,y_i) \cos\left[\Theta_p(x_i,y_i) + \frac{2\pi(n-1)}{p} \right] \end{aligned} \tag{14}$$

where

$$\begin{aligned} \mathscr{A}_p(x_i,y_i) &= E_r^2 + \left| U_{i_p}^{(1)}(x_i,y_i) \right|^2, \\ \mathscr{B}_p(x_i,y_i) &= 2E_r \left| U_{i_p}^{(1)}(x_i,y_i) \right|^2, \\ \Theta_p(x_i,y_i) &= \arg\left[U_{i_p}^{(1)}(x_i,y_i) \right]. \end{aligned} \tag{15}$$

Eq. (14) is the classic interference expression, where the rotation of the MSSPF is all but a piston term in the interferogram. As the rotation of the filter can be done only in equispaced increments (unlike continuous spiral phase plate), analytic signal of the n-interferograms, for $p \geq 3$ can be calculated using [15],

$$U_{i_p}^{(1)}(x_i,y_i) = \sum_{n=1}^{p} I_p^{(n)}(x_i,y_i) \exp\left[i\frac{2\pi(n-1)}{p} \right] \tag{16}$$

The extracted parameters are convolved with the MSSPF kernel. Therefore, a deconvolution process has to be applied.

$$U_o(x_i,y_i) = U_{i_p}^{(1)}(x_i,y_i) \otimes h_p^{-1}(x_i,y_i). \tag{17}$$

The symbol $\otimes$ stands for the convolution operation and $h^{-1}(x_i,y_i)$ is the inverse of the kernel of the MSSPF, which is a function that has the property of $\mathbb{H}_p^{(1)}(u,v)\mathbb{H}_p^{(1)^{-1}}(u,v) = 1$. This can be easily done because it is a phase filter, when the MSSPF is elevated to the power $^{-1}$ the phase of the filters cancel and the deconvolution process can be carried out.

The phase increments introduced by the displacement of the object at the image fields are approximately equal at conjugate points $(x_i,y_i) = (Mx_o, My_o)$, where M is the magnification of

#204866 - $15.00 USD Received 27 Jan 2014; revised 13 Mar 2014; accepted 15 Mar 2014; published 2 Apr 2014

the system, and is equal to -1 in the case of a $4f$ correlator. Therefore the phase increment that we sought is given by

$$\varphi_o^{(e)}(x_o,y_o) \simeq \arg\left[U_o(-x_i,-y_i)\right], \tag{18}$$

where the superscript e stands for extracted.

3. Numerical simulation of phase extraction with a Mach-Zender interferometer

To verify the phase extraction Eqs., a numerical simulation of a Mach-Zehnder interferometer in a MSSPF configuration was devised. Depending on the magnitude of the phase introduced by the objects under analysis by the proposed technique, two different scenarios can be anticipated for the kind of interferograms obtained with the proposed technique: first, when the object phases have values $\geq 2\pi$ producing fringes that do not exceed the Nyquist sampling limit, in this case a typical interferogram depicts spiral fringe patterns for smooth phase changes. On the other hand, when the object phases are weak e.g. as occur in Zernike phase contrast microscopy, only an edge enhancement effect can be observed instead of fringe patterns. The numerical simulations of these two scenarios are presented next, to show that phase extraction with the proposed method is effective for weak and non-weak phase magnitudes.

3.1. Spiral fringe patterns

In order to make the numerical simulation preliminary values for the amplitude $E_o(x_o,y_o)$ and phase $\varphi_o(x_o,y_o)$ of the object field were defined, where the maximum value of the phase corresponded to 6π. The field $U_{i_p}^{(n)}(x_i,y_i)$ at the image plane of the $4f$ correlator shown in Fig. 3 was obtained after two numerical Fourier transformations, indicated in Eq. (10) using $p=4$. After computing this field, the intensity resulting from the superposition of $U_{i_p}^{(n)}(x_i,y_i)$ and a plane wave of constant amplitude E_r and zero phase is found. As a result of this numerical simulation, the intensity distribution $I_4^{(n)}(x_i,y_i)$ in Fig. 4 shows the result of this operation. It can be seen that a spiral carrier is obtained as for the continuous spiral phase plate. Unlike continuous spiral phase plate, an extra diffraction pattern caused by the incomplete doughnut kernel of the continuous spiral phase plate can be noticed. Using Eq. (16) and (17) the convolved and

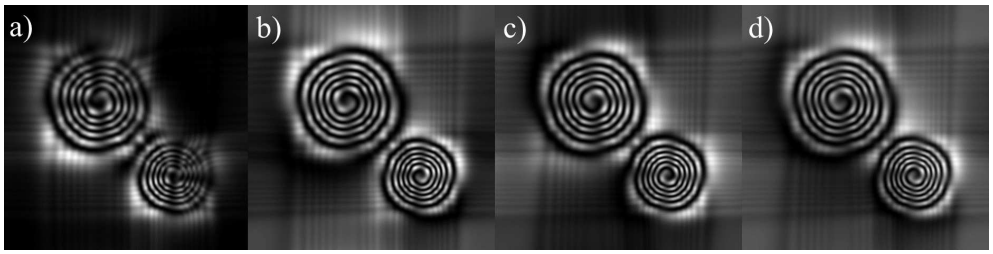

Fig. 4. Computed Interference pattern for $p=4$, a) $I_4^{(1)}(x_i,y_i)$, b) $I_4^{(2)}(x_i,y_i)$, c)$I_4^{(3)}(x_i,y_i)$, d)$I_4^{(4)}(x_i,y_i)$ of a double element phase object

deconvolved phase are extracted using the interference patterns shown in Fig. 4.

3.2. Phase contrast patterns

In order to illustrate the effect of this method when an weak phase object ($\ll 2\pi$), numerical simulation was carried out. We have then defined the preliminary values for the amplitude $E_o(x_o,y_o)$ and phase $\varphi_o(x_o,y_o)$ of the object field, where the maximum value of the phase corresponded to 0.1π. For this simulation, an USAF optical test pattern was used as the phase object

#204866 - $15.00 USD Received 27 Jan 2014; revised 13 Mar 2014; accepted 15 Mar 2014; published 2 Apr 2014

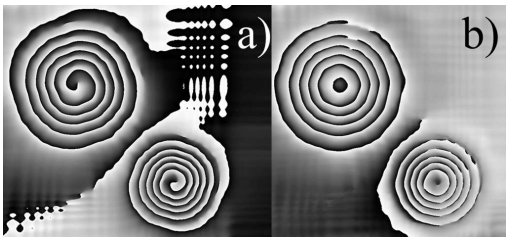

Fig. 5. Extracted wrapped phase using the interferograms of Fig. 4. a) Convolved phase $\Theta_4(x_i,y_i)$, b) Deconvolved phase $\varphi_o^e(x_o,y_o)$

$\varphi_o(x_o,y_o)$. As for the strong phase object simulation the field $U_{i_p}^{(n)}(x_i,y_i)$ at the image plane of the $4f$ correlator shown in Fig. 3 was obtained after two numerical Fourier transformations, indicated in Eq. (10) using $p=4$. After computing this field, the intensity resulting from the superposition of $U_{i_p}^{(n)}(x_i,y_i)$ and a plane wave of constant amplitude E_r and zero phase is found. As a result of this numerical simulation, the intensity distributions $I_4^{(n)}(x_i,y_i)$ were calculated, this interferograms can be seen in Fig. 5.

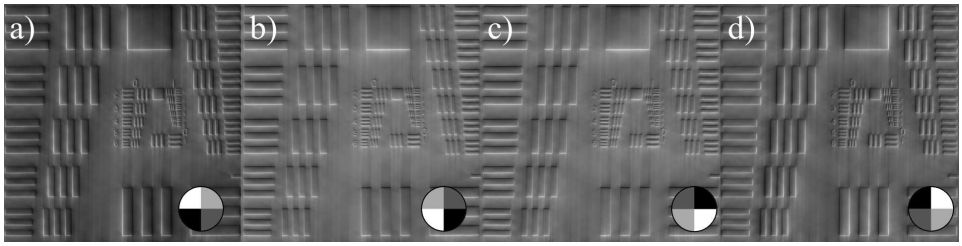

Fig. 6. Computed Interference pattern for $p=4$, a) $I_4^{(1)}(x_i,y_i)$, b) $I_4^{(2)}(x_i,y_i)$, c)$I_4^{(3)}(x_i,y_i)$, d)$I_4^{(4)}(x_i,y_i)$ of an only phase USAF optical test pattern

It can be seen that there is no spiral carrier in the interferograms, but an edge enhancement of the object is obtained. This effect is the same as the one obtained using the continuous spiral plate [9]. So this technique can be applied in spiral phase contrast microscopy, allowing the implementation of the MSSPF in a quantitative phase contrast microscopy. The phase can be extracted implementing Eqs. (16) and (17) using the interference patterns shown in Fig. 6. The extracted phase is displayed in Fig. 7.

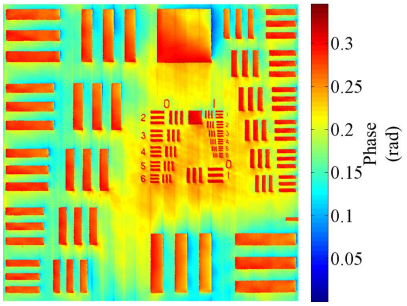

Fig. 7. Extracted phase using the interferograms of Fig. 6.

#204866 - $15.00 USD Received 27 Jan 2014; revised 13 Mar 2014; accepted 15 Mar 2014; published 2 Apr 2014

3.3. *Influence of the number of steps in the residual noise*

To test the reliability of this method, we made use of the Universal Quality Image Index Q, which provides a measure of the similitude of two gray level images [16]. It is given by the expression

$$Q = \frac{\sigma_{xy}}{\sigma_x \sigma_y} \frac{2\overline{xy}}{\overline{x}^2 + \overline{y}^2} \frac{2\sigma_x \sigma_y}{\sigma_x^2 + \sigma_y^2} \tag{19}$$

where $\overline{x}$ and $\overline{y}$ are the average of Nth dimensional vectors $\mathbf{x}$ and $\mathbf{y}$ and σ_x^2, σ_y^2, and σ_{xy} are the co-variances of these vectors. The range of Q is$[-1,1]$, then if $Q = 1$, the images are exactly the same. The Q index is used to compare the extracted phase and the original simulated phase. The extracted analyzed phase was unwrapped by following [17] as shown in Fig. 8(a), and then Q was calculated using Eq. (19). To illustrate the error generated by the extracted phase, an

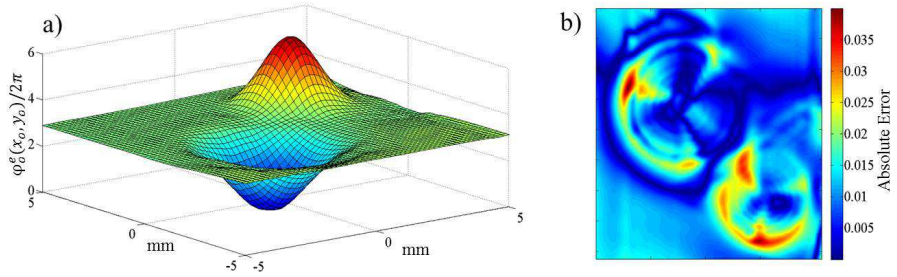

Fig. 8. a) Unwrapped extracted phase, b) Absolute error map, between the unwrapped extracted phase and the simulated phase

absolute error map is shown in Fig. 8(b). Nevertheless to make an accurate comparison Q was used obtaining the results can be seen in Table 1.

Table 1. Dependance of the Quality index and the number of steps of the MSSPF

p	Q
3	0.884
4	0.905
5	0.912
6	0.912
7	0.913
8	0.914
10	0.914
20	0.915

It can be seen that starting with the three-steps of the MSSPF, the quality index is already high enough, therefore the approximation to the phase is of good quality for high speed acquisition purpouses. A low number of steps, mean that faster interferogram acquisition can be achieved by rotating the MSSPF in shorter times, therefore it can be used for objects who might change quickly by reducing the number of interferograms. For steps greater than three, the quality index shown in table 1 remain almost the same, but with a slight increment as the number of steps grow. It is worth pointing out that a residual error is present in the extracted phase despite

#204866 - $15.00 USD Received 27 Jan 2014; revised 13 Mar 2014; accepted 15 Mar 2014; published 2 Apr 2014

the addition of more steps to the method. Figure 8(b) shows the absolute error obtained for the four-steps MSSPF, when the phase of Fig. 8(a) is processed by the Mach-Zender simulation. It can be seen that the largest error (up to 4%) is present in the borders of the phase. This error magnitude has been reported previously using other extraction methods, but with continuous spiral fringe demodulation techniques [18, 19].

4. Experimental results

Figure 9 shows the experimental setup for the phase extraction of a phase object using the MSSPF. The light from a He-Ne Laser L ($\lambda = 632.8$ nm) is expanded using a microscope objective *MO* and collimated by the lens L_0. The light is divided by a beam splitter BS_1 into a reference beam (shown as dashed line) and the object beam (presented with a dotted line). The phase object *Ob* is a biconvex lens of 6 mm diameter. The examined area is 10×12 mm. The object is placed at the back focal plane of the lens L_1, with 400 mm focal length and 35 mm diameter. The LCoS model LC-R 2500 by Holoeye ™, is placed at the back focal plane of L_2, both L_1 and L_2 are identical. The light reflected by the LCoS is collected by the lens L_2 which incides directly into the CCD. The reference beam, generated by the reflection of light in the beam splitter BS_1, is directed to the beam splitter BS_3 by mirror M_1. Finally the interference pattern of reference and object beams is recorded by the CCD.

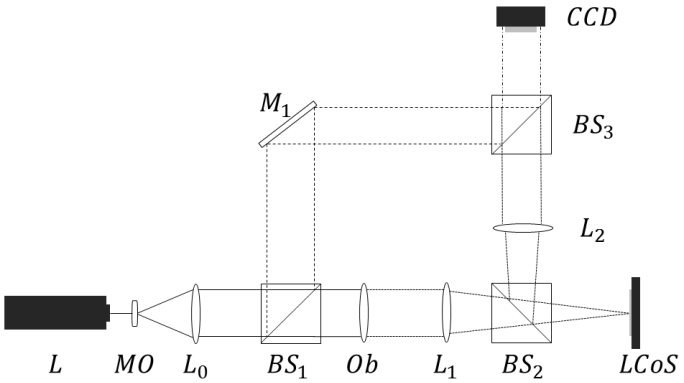

Fig. 9. Schematic Diagram of the experimental Setup. A detailed description of the elements and their function is given in the text.

The LCoS has been previously calibrated to display the corrected steps by using the LCoS shape and a corrected polarization for the laser wavelength of the experiment, otherwise the spiral carrier is transformed to arbitrary phase values determined by the particular LCoS polarization and shape. From previous calibration work [20, 21], it was also shown that the model of LCoS used in our experiment can not achieve a full dynamic range of 2π, so the number of steps of the MSSPF were limited by the maximum allowable phase range. It is worth pointing out, that given the limited range of our SLM, a continuous spiral phase plate can not be displayed. Figure 10 shows the experimental interference pattern $I_p^{(n)}(x_i, y_i)$ obtained with the experimental setup of Fig. 9. Three different filters were tested to prove the effectiveness of the technique $p = 3, 4, 5$. The obtained interferograms are presented in Fig. 10, where it can bee seen that the spiral carrier is preserved but with an additional spurious diffraction pattern.

Using the captured sequence $I_4^{(1)}(x_i, y_i)$, $I_4^{(2)}(x_i, y_i)$, $I_4^{(3)}(x_i, y_i)$ and, $I_4^{(4)}(x_i, y_i)$, and using Eq. (16) the convolved wrapped phase can be extracted; the result is shown in Fig. 11(a). The deconvolution process of the phase is applied next, to obtain the wrapped phase shown in Fig. 11(b).

#204866 - $15.00 USD Received 27 Jan 2014; revised 13 Mar 2014; accepted 15 Mar 2014; published 2 Apr 2014

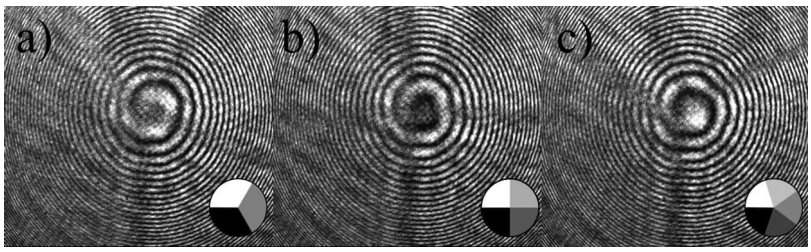

Fig. 10. Experimental Interference pattern $I_p^{(n)}(x_i,y_i)$ with the MSSPF gray representation in the right corner. a) $I_3^{(1)}(x_i,y_i)$, b) $I_4^{(1)}(x_i,y_i)$, c) $I_5^{(1)}(x_i,y_i)$

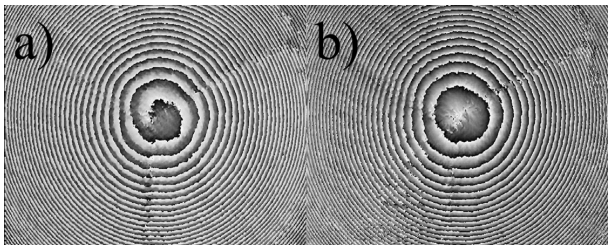

Fig. 11. Experimental extracted wrapped phase. a) Convolved phase $\Theta_4(x_i,y_i)$, b) Deconvolved phase $\varphi_o^e(x_o,y_o)$

The technique performance on measurement presicion, was also evaluated using the quality index, but now using the resulting phase of the proposed method and the phase values obtained by a Wyco ^{TM} interferometer with the same object under study. The resulting quality index for the experimental results are amost equal to the simulated results for the three-steps MSSPF: $Q = 0.847$, however there is a slight decrement of quality index if a four-steps MSSPF is used: $Q = 0.898$. The best experimental performance was obtained using the five-steps MSSPF: $Q = 0.902$. Greater number of steps were not implemented in our experiment due to the restricted dynamic range of the SLM model used in the experiment.

5. Conclusions

In conclusion, we presented an alternative method for phase extraction from interferograms obtained with multi-step spiral phase filter (MSSPF). The phase extraction is based on the rotation of the MSSPF, which can be achieved easily with a spatial light modulator (SLM). This method has some advantages over traditional single-shot spiral interferometry. This technique can also be used for phase extraction of weak phase objects where no spiral fringes are produced in the interference patterns. This leads to a quantitative phase contrast method for any kind of phase objects; as a tradeoff this phase extraction technique requires several interferograms corresponding to the rotations of the filter. Unlike the continuous spiral phase filter the MSSPF dynamic range depends directly on the number of steps of the filter, therefore the MSSPF can be displayed in an SLM with dynamic range smaller than 2π. Nonetheless the reduced phase modulation, spiral fringe are still obtained in the interferograms which can be used with the proposed phase extraction method. The calibration of SLM is easier as it only consists of fixing a reduced number of phase steps, avoiding detuning of a large set of steps required for a continuous vortex generation. Compared to PZT transducers, there is no hysteresis. Not only twisted nematic nor parallel aligned SLM can be used but also binary SLM, due to the intrinsic discontinuity of the MSSPF. An additional advantage of the proposed method is that most of the reported techniques use the first diffraction order to introduce the vortex, however this method introduces the vortex in the zero order with increased light efficiency. It is also shown that the proposed method gives a phase reconstruction with residual noise depending on the number of steps, with similar noise values for steps greater than or equal to four. This technique can also

#204866 - $15.00 USD Received 27 Jan 2014; revised 13 Mar 2014; accepted 15 Mar 2014; published 2 Apr 2014

be extended to MSSPF with different topological charges, except that the topological charge will affect the distribution of the spiral fringes. Nonetheless the phase remains embedded in the new distribution of the generated fringes, therefore by using the MSSPF corresponding deconvolution kernel, it can be seen that the phase can be retrieved using a similar approach.

Acknowledgments

Alberto Aguilar would like to thank CONACyT for financial support. Also, the authors would like to thank Daniel Malacara Doblado and David Moreno Hernández for supplying some equipment required for this work.

#204866 - $15.00 USD Received 27 Jan 2014; revised 13 Mar 2014; accepted 15 Mar 2014; published 2 Apr 2014